

Electronic Supporting Information

Low Temperature and Limited Water Activity Reveal a Pathway to Magnesite via Amorphous Magnesium Carbonate

Sebastian T. Mergelsberg^a, Sebastien N. Kerisit^a, Eugene S. Ilton^a, Odeta Qafoku^b, Christopher J. Thompson^c, and John S. Loring^{*a}

^a Physical and Computational Sciences Directorate, Pacific Northwest National Laboratory, Richland, WA 99354, United States E-mail: john.loring@pnnl.gov

^b Earth and Biological Sciences Directorate, Pacific Northwest National Laboratory, Richland, WA 99354, United States

^c Energy and Environment Directorate, Pacific Northwest National Laboratory, Richland, WA 99354, United States

*. Corresponding Author: john.loring@pnnl.gov

Methods

Materials. Nanosized forsterite (Mg_2SiO_4), with a nitrogen Brunauer-Emmet-Teller¹ (BET) determined specific surface area of $43.3 \text{ m}^2/\text{g}$, was used in this investigation. The synthesis and characteristics of the forsterite have previously been described in detail by Qafoku et al.² Carbon dioxide purchased from Oxarc Inc. with a purity $>99.999\%$. Reagent water was de-ionized (Barnstead NanoPure) and had a resistivity of $18.2 \text{ M}\Omega\cdot\text{cm}$. All materials for the synthesis of AMC were from Sigma-Aldrich: $\text{MgCl}_2\cdot 6\text{H}_2\text{O}$ ($\geq 99\%$), methanol (HPLC grade, $\geq 99\%$), Cs_2CO_3 (99%), and acetone (HPLC grade, $\geq 99.9\%$).

***In situ* High-Pressure Infrared Spectroscopic Titrations.** *In situ* high-pressure IR titrations with H_2O were carried out in liquid CO_2 at $25 \text{ }^\circ\text{C}$ and 90 bar using an automated fluid-delivery apparatus coupled to a custom-built high-pressure IR reaction cell with both transmission and attenuated total reflection (ATR) IR optics.³⁻⁵ IR spectra were collected using a Bruker Vertex 80V spectrometer equipped with an air-cooled source, deuterated tri-glycine sulfate (DTGS) detector, and housed in an environmental chamber thermostated to $25\pm 0.2 \text{ }^\circ\text{C}$. The high-pressure optical cell holds a volume of 62.2 mL and is jacketed for temperature control by a circulating water bath. Temperature is monitored by a high-pressure, K-type thermocouple that is positioned within the main fluid cavity of the cell and that was calibrated using ice and boiling water. Cell pressure is monitored by a pressure transducer that was calibrated against a NIST-traceable standard gauge. The transmission IR optics consist of cylindrical ZnSe windows and a pathlength of $\sim 4 \text{ cm}$. The internal reflection element (IRE) of the ATR IR optics is a single-reflection 45° prism made of ZnSe (Harrick Scientific). A detailed description of the fluid delivery apparatus, reaction cell, spectrometer settings, spectral collection procedures, titration loop calibrations, the general method for performing titrations, and data analysis procedures have been described in detail elsewhere³⁻⁵.

During a typical titration, transmission IR and ATR-IR spectra were acquired as a function of H_2O addition and time. After cell pressurization with CO_2 , a tubing loop with a calibrated volume was used to meter water into the cell to increase fluid percent H_2O saturation stepwise. (Note that we use the term “percent H_2O saturation” in this study because CO_2 at $25 \text{ }^\circ\text{C}$ and 90 bar is a liquid. Otherwise, if the conditions had been such that the CO_2 was a gas or a supercritical fluid, we would have used the term “relative humidity”.) A reaction time of 135 minutes was used between H_2O additions. Transmission IR spectra were of the wet liquid CO_2 , and their background spectrum was of the anhydrous fluid. These spectra were processed in the HOH bending mode region of dissolved H_2O to determine fluid percent H_2O saturation and the amount of H_2O adsorbed onto the forsterite. ATR-IR spectra were of forsterite, and their background spectrum is of the empty cell under vacuum (10^{-3} Torr). These spectra are collected to follow the reactivity of forsterite towards carbonation.

Four IR experiments were performed and summarized in Table S1: (1) a calibration, 25C_Cal (2) a titration, 25C_Titra, (3) a time dependent experiment, 25C_Time_Dep, and (4) an experiment to generate magnesite and amorphous SiO_2 standards, 50C_Fully_React. The first three experiments are described here, while 50C_Fully_React is explained in the “AMC, Magnesite, and Amorphous SiO_2 Standards” section below. The calibration, 25C_Cal, was carried out to determine the correlation between the concentration of dissolved H_2O in the fluid (i.e., percent H_2O saturation)

and the absorbance of its HOH bend, as well as to measure the concentration of H₂O dissolved in liquid CO₂ at saturation. This experiment was performed by titrating H₂O into the pressurized cell in the absence of forsterite. Transmission IR was used to correlate the absorbance of the HOH bend of H₂O to H₂O concentration in the fluid; the concentration of H₂O at saturation was 56 ± 1 mM, in reasonable agreement with a value of 57.4 mM predicted by the model of Spycher et al.⁶ The purpose of the titration, 25C_Titra, was to determine the amount of H₂O adsorbed on forsterite as a function of percent H₂O saturation. For this experiment, H₂O was titrated into the pressurized cell containing 0.22067 g of forsterite evaporated onto a microscope slide from a suspension in isopropanol. Adsorbed H₂O concentrations were calculated from the difference between the known amount of H₂O added to the cell and the measured amount of H₂O dissolved in the fluid. H₂O coverages in ML were determined using molecular dynamics-derived parameters from Kerisit et al. for the (010) forsterite surface^{7, 8}. The time dependent experiment, 25C_Time_Dep, was carried out to follow the carbonation of forsterite as a function of time at a constant percent H₂O saturation. In this experiment, 0.1 mL of a ~5 g/L forsterite suspension in isopropanol was evaporated onto the IRE to form an ATR overlayer, and an additional 0.1 mL of this suspension was evaporated onto a glass microscope slide to be used later for SEM analysis. H₂O was titrated into the cell until a target H₂O coverage on the forsterite was reached, and then spectra were collected as a function of time to follow the carbonation of the forsterite. ATR-IR spectra from the time dependent experiment were corrected for distortions^{9, 10} by first converting to optical constant spectra using the method of Bertie et al.^{11, 12}, followed by calculating absorbance spectra from these optical constants for a hypothetical 1 μm pathlength transmission cell using the Fresnel equations.^{13, 14}

The ATR distortion corrected spectra from the time dependent experiment, 25C_Time_Dep, was analyzed to follow (a) carbonate growth and (b) forsterite dissolution. Carbonate growth was monitored in both the CO deformation (715 to 770 cm⁻¹) and asymmetric CO stretching (1215 to 1600 cm⁻¹) regions. The spectrum at 0% H₂O saturation was subtracted from each measured spectrum; thus, the background spectrum in this analysis is that of the unreacted forsterite at pressure and temperature. The spectra were baseline corrected in the CO deformation region by subtracting the line fit to absorbances from 705 to 715 cm⁻¹ and 760 to 770 cm⁻¹; and in the asymmetric CO stretching region by subtracting the line fit to absorbances from 1240 to 1250 cm⁻¹ and 1870 to 1900 cm⁻¹. Absorbances between 770 and 1220 cm⁻¹, were set to zero, and then a singular value decomposition was performed between 703 and 1894 cm⁻¹. Two eigenvectors from this analysis accounted for 99.96% of the variance in the data, and this indicates that the measured spectra can be accounted by two physically-real component spectra. One of these components was assumed to be amorphous magnesium carbonate (AMC), which demonstrates no obvious CO deformation band between 715 and 770 cm⁻¹; while the other component was assumed to be magnesite, which has a weak by obvious deformation band at 746 cm⁻¹.^{15, 16} These eigenvectors were coadded to produce a spectrum assigned to AMC that had minimum absorbance between 715 and 770 cm⁻¹. Finally, a 2-component multivariate curve resolution-alternating least squares (MCR-ALS) chemometrics analyses was performed on the data 703 and 1894 cm⁻¹. By default, this analysis uses a non-negativity constraint in both spectral and concentration space.¹⁷⁻¹⁹ However, an additional constraint was applied that one of the components, C1, was fixed to the spectrum of AMC derived from the coaddition of the SVD eigenvectors. The MCR-ALS analysis solved for the second component, C2, which we assign to the spectrum of magnesite, and it also calculated the relative concentrations of both C1 and C2 as a function of time.

Forsterite dissolution (as well as amorphous SiO₂ precipitation) was monitored in the in the SiO stretching region of amorphous SiO₂ (1060 to 1130 cm⁻¹) and forsterite (970 to 1060 cm⁻¹). The background spectrum for each measured spectrum was the empty cell, and spectra of the unreacted forsterite at 0% H₂O saturation were included in the analysis. Spectra were baseline corrected by subtracting the average of the absorbances between 1177 and 1207 cm⁻¹ from the absorbances below 1220 cm⁻¹. A 2-component MCR-ALS analysis was then performed with the constraint that one of the components, S1, was fixed to the spectrum of the unreacted forsterite. The MCR-ALS analysis solved for the second component, S2, which we assign to the spectrum of reacted forsterite, and it also calculated the relative concentrations of both S1 and S2 as a function of time.

AMC, Magnesite, and Amorphous SiO₂ Standards. AMC was synthesized using a procedure similar to Leukel et al.²⁰ 2 mM MgCl₂ · 6 H₂O was reacted with 2 mM Cs₂CO₃ in 20 mL methanol with sonication for 1 min. A white solid (AMC) precipitated and was collected by centrifugation. The solid was washed twice with 10 mL methanol to remove the residual cesium chloride, then twice with 20 mL acetone. Finally, the precipitate was dried under N₂ at room temperature. Finally, a 0.1 mL of a ~5 g/L suspension of AMC in isopropanol was evaporated onto the ZnSe IRE of the high-pressure IR titration cell (see above) to form an overlayer, and an ATR IR spectrum was collected. This sample was also analyzed using heXRD (see below).

An IR titration experiment, 50C_Fully_React (see above and Table S1), was carried out to generate a sample comprised of magnesite and amorphous SiO₂ products forsterite carbonation that could be used as standards for IR, as well as heXRD (see below). In this experiment, forsterite was reacted in supercritical CO₂ (scCO₂) at 50 °C, 90 bar, and 100% percent H₂O saturation (i.e., relative humidity) in the high-pressure IR titration cell. 100% percent H₂O saturation was achieved by titrating excess water into the cell required to saturate the scCO₂. We roughly estimated that hundreds of monolayers of H₂O condensed onto the forsterite, and we thus consider this a bulk H₂O experiment. This estimate was made by quantitative comparison of the HOH stretching bands of adsorbed H₂O in ATR IR spectra of the reacting forsterite to those spectra from other titrations we have performed of forsterite carried out at this temperature and pressure where H₂O coverage is determined by the transmission IR data.²¹ ATR IR spectra were collected as a function of time for two days to follow the consumption of forsterite and the formation of a magnesium carbonate precipitate and amorphous SiO₂. Forsterite SiO stretching bands were not observed after 32 hours. The cell was depressurized and evacuated, and then an ex situ ATR IR spectrum was collected. The postreacted sample was collected from the IRE and analyzed by heXRD (see below), confirming that the carbonate that formed was magnesite with no other hydrated carbonate phases present (e.g., AMC or nesquehonite, MgCO₂ · 3H₂O).

SEM Imaging. SEM measurements were performed on the post-reacted forsterite on the glass slide from Titration #3 (see above). Images were collected using a Helios NanoLabTM 600i from FEI. The sample was coated with a 10 nm thick C layer to reduce sample charging.

XRD and PDF Characterization. High energy X-ray diffraction and total X-ray scattering for PDF analysis was carried out on the post-reacted forsterite scraped from the IRE from Titration #3 (see above). Data were collected at beamline 11 ID-B of the Advanced Photon Source,²² Argonne National Laboratory (Argonne, IL, USA) during top-up mode (58.66 keV, λ = 0.2113 Å), using an amorphous silicon-based Perkin-ElmerTM detector (2048x2048 pixel resolution, 200x200 μm² pixel size). Instrument parameters were calibrated using a cerium dioxide standard (CeO₂, NIST

diffraction intensity standard set 674a, diluted 1:25 with glassy carbon). Powder samples were loaded into 0.8 mm inner diameter polyimide (Kapton®) capillaries and sealed with general purpose epoxy (Devcon, 5 Minute® Rapid-Curing). Total scattering scans were the summation of 400 exposures of 0.75 sec length collected at 158 mm sample-to-detector distance. High-energy x-ray diffraction was measured by summing 300 exposures of 2 sec duration at a distance of 800 mm. Dark images matching the data acquisition frame rate were acquired in 5 min intervals and subtracted from active scans to remove detector noise. Dead and overexposed pixels on the detector were masked in General Structural Analysis System II. (GSAS-II).²³ Rietveld refinement of heXRD data was performed in GSAS-II using the chebyshev-1 algorithm with 9 terms to fit the background. Instrument parameters were refined using diffraction of the CeO₂, NIST diffraction intensity standard set 674a. Unit cell parameters, particle sizes, and particle strain were refined using previously published forsterite and magnesite structures.^{24, 25} Pair Distribution Function (PDF) profiles were calculated in PDFgetX3 (Columbia Technology Ventures).

To determine the instrument parameters necessary for fitting the data, a ceria standard (CeO₂) was first measured and refined for both heXRD refinements and analysis of the pair distribution function (PDF, Fig. S5). Lattice parameters of forsterite and magnesite were then refined by fitting the PDF patterns of unreacted forsterite and the magnesite precipitated in experiment 50C_Fully_React (see above and Table S1), respectively (Figure S6). Using the refined unit cells parameters, the average forsterite domain size was determined to be 45 nm, which is approximate agreement with the particle sizes determined from SEM. The poor fit of forsterite and magnesite to the PDF is due to the sensitivity of the technique to the formation of amorphous SiO₂ and AMC. Note that all fits and refinements yield vol%, not the reported mol%. Because the hydration state of amorphous silica and AMC in the experiment are unknown, the calculation to convert from the refined vol% to mol% was performed assuming molar densities of the most and least hydrated forms of silica and the calcium analogue of AMC, amorphous calcium carbonate (ACC), reported in the literature (Table S2).²⁶⁻²⁸ These are termed “wet” and “dry” fits, respectively.

Table S1: Experiments, Techniques and Conditions, and Purpose.

Experiments	Techniques and Conditions	Purpose
	<u>25°C Calibration</u>	
25C_Cal	Transmission IR from <i>in situ</i> IR spectroscopic titration in the absence of forsterite in liquid CO ₂ at 25°C and 90 bar	Correlate integrated absorbance of HOH bend to dissolved H ₂ O concentration; Determine concentration of H ₂ O required to saturate fluid
	<u>25°C Titration</u>	
25C_Titra	Transmission IR from <i>in situ</i> IR spectroscopic titration of forsterite in liquid CO ₂ at 25°C and 90 bar	Correlate H ₂ O coverage on forsterite to percent H ₂ O saturation of the fluid
	<u>25°C Time Dependent Experiment</u>	
25C_Time_Dep	ATR IR from <i>in situ</i> IR spectroscopic titration of forsterite in liquid CO ₂ at 25°C and 90 bar, but as function of time after reaching 64% H ₂ O saturation (H ₂ O coverage of 1.82 ML); <i>Ex situ</i> heXRD, and SEM characterization	Identify carbonation products; model carbonation kinetics
	<u>50°C Forsterite Fully Reacted in Bulk Water Experiment</u>	
50C_Fully_React	ATR IR from <i>in situ</i> IR spectroscopic titrations and <i>ex situ</i> heXRD of forsterite fully reacted in bulk H ₂ O (100% relative humidity) to amorphous SiO ₂ and magnesite at 50°C and 90 bar	Generate IR and heXRD standards for magnesite and amorphous SiO ₂

Table S2. Refinement results from heXRD and PDF fitting.^a

refinement	Forsterite (mol%)	Magnesite (mol%)	SiO ₂ (mol%)	AMC (mol%)	Adj. R ²	Red. χ^2	R _{wp} (%)
PDF “dry”	72.87 ± 0.24	1.53 ± 0.11	10.57 ± 0.37	15.03 ± 0.12	0.8285	0.20712	
PDF “wet”	80.35 ± 0.27	1.69 ± 0.12	7.76 ± 0.27	10.20 ± 0.08	0.8285	0.20712	
XRD Rietveld	98.30 ± 0.44	1.70 ± 0.23	--	--	--	0.00092	2.70

^a Both refinements quantify the vol% of each component. Conversion into mol% was performed assuming the molar density of fully hydrated (wet) and least hydrated (dry) amorphous products. Results of PDF fit are shown in Figure 3A and the XRD Rietveld refinement is shown in Figure S6A.

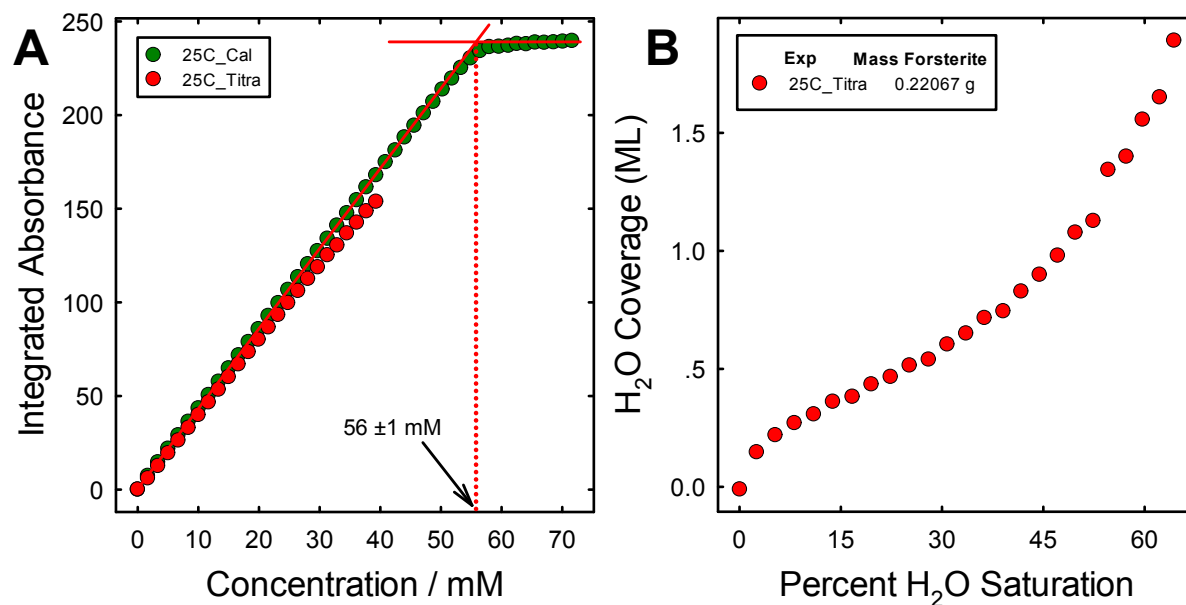


Figure S1. (A) Integrated absorbance of the HOH bending mode of dissolved H₂O versus total H₂O concentration from experiments 25C_Cal and 25C_Titra (see Table S1) in liquid CO₂ at 90 bar and 25 °C. The intersection of the straight lines fit through the linear and plateau regions of the data is the dissolved H₂O concentration at saturation. (B) H₂O coverage as a function of percent H₂O saturation for the titration of 0.22067g forsterite with H₂O in liquid CO₂ at 90 bar and 25°C (experiment 25C_Titra; see Table S1). We estimate the uncertainty in the H₂O coverage to be 0.1 ML.

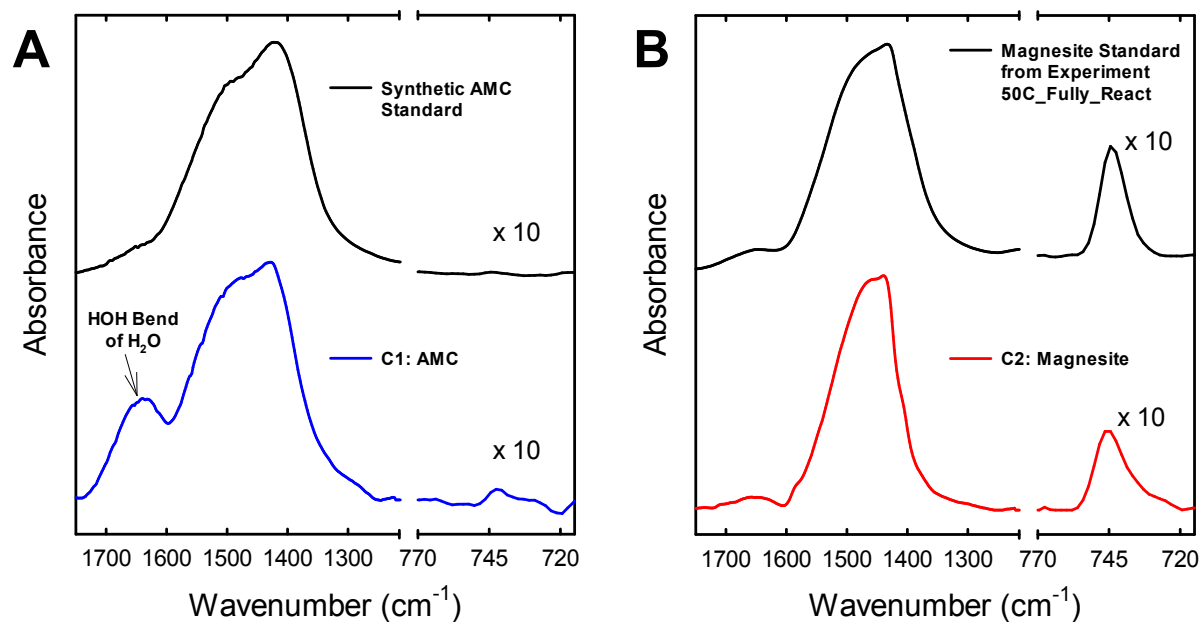


Figure S2. (A) Spectral component C1 compared to a spectrum of a synthetic AMC standard, and (B) component C2 compared to a spectrum of magnesite from experiment 50C_Fully_React (see Table S1), in CO deformation (715 to 770 cm^{-1}) and asymmetric CO stretching (1215 to 1600 cm^{-1}) regions of carbonate. Components C1 and C2 are from the MCR-ALS analysis of ATR IR spectra from experiments 25C_Time_Dep, 40C_Time_Dep, and 50C_Time_Dep (see Table S1), as described in the main text and Supporting Information. The spectrum of the AMC standard is a distortion corrected ATR spectrum of AMC that was synthesized as described in the Methods section. The spectrum of magnesite is a distortion corrected ATR spectrum of forsterite fully reacted in wet CO_2 in bulk H_2O (100% percent H_2O saturation) at 50 °C and 90 bar.

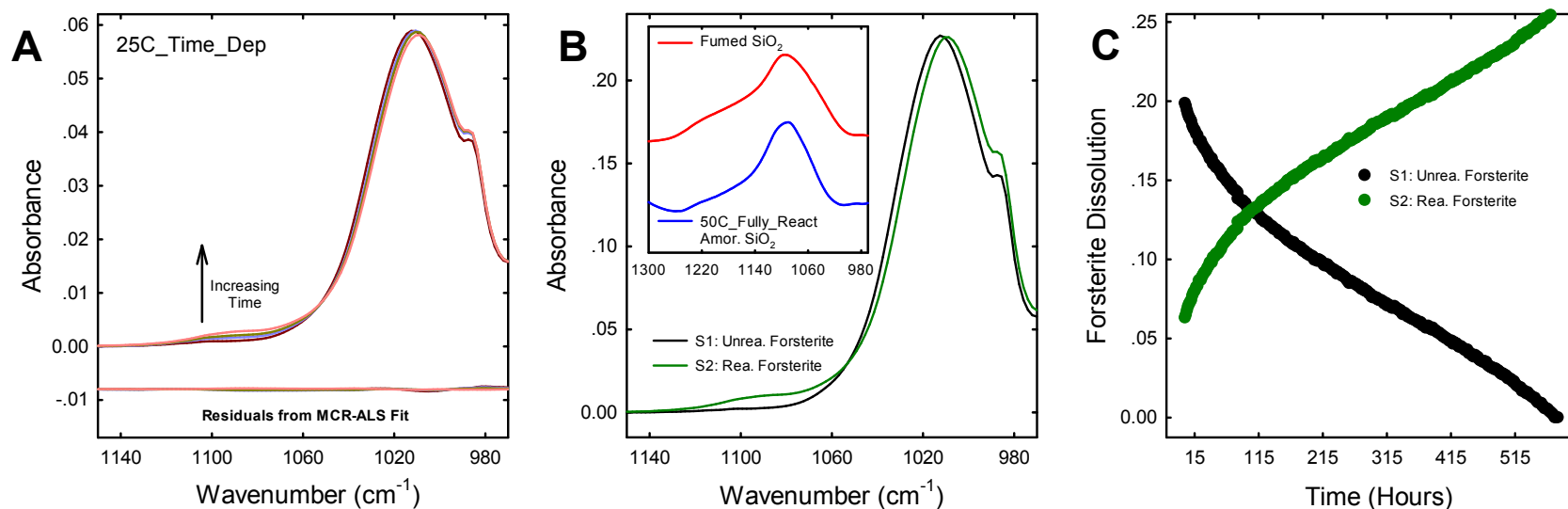


Figure S3. (A) Examples of the ATR IR spectra in the SiO stretching regions of amorphous SiO₂ (1060 to 1130 cm⁻¹) and forsterite (970 to 1060 cm⁻¹) as a function of time after reaching 64% H₂O saturation (a H₂O coverage of 1.82 ML) during experiment 25C_Time_Dep (see Table S1), in which forsterite was titrated with H₂O in liquid CO₂ at 25 °C and 90 bar. Spectra are at 194 hour increments from 0 to 582 hours, and their background spectrum is the empty cell. The baseline corrected spectra were fit using a two-component MCR-ALS analysis that accounted for 99.99% of the variance, and examples of residuals are shown offset and below the measured spectra. The two spectral components, S1 and S2, are shown in (B) and assigned to unreacted and reacted forsterite, respectively. To support the interpretation that the absorbance between 1060 to 1130 cm⁻¹ is due to precipitated amorphous SiO₂, the inset in panel B shows an ATR IR spectrum of fumed silica (Aldrich)²⁹ and the *ex situ* ATR IR spectrum from experiment 50C_Fully_React (see Table S1) in the SiO stretching region. The MCR-ALS derived relative concentrations of components S1 and S2 as a function time are shown in (C). The lines are fits to the data according to the kinetics model as described in the main text. Details of spectral processing and chemometrics analyses are in the methods section above.

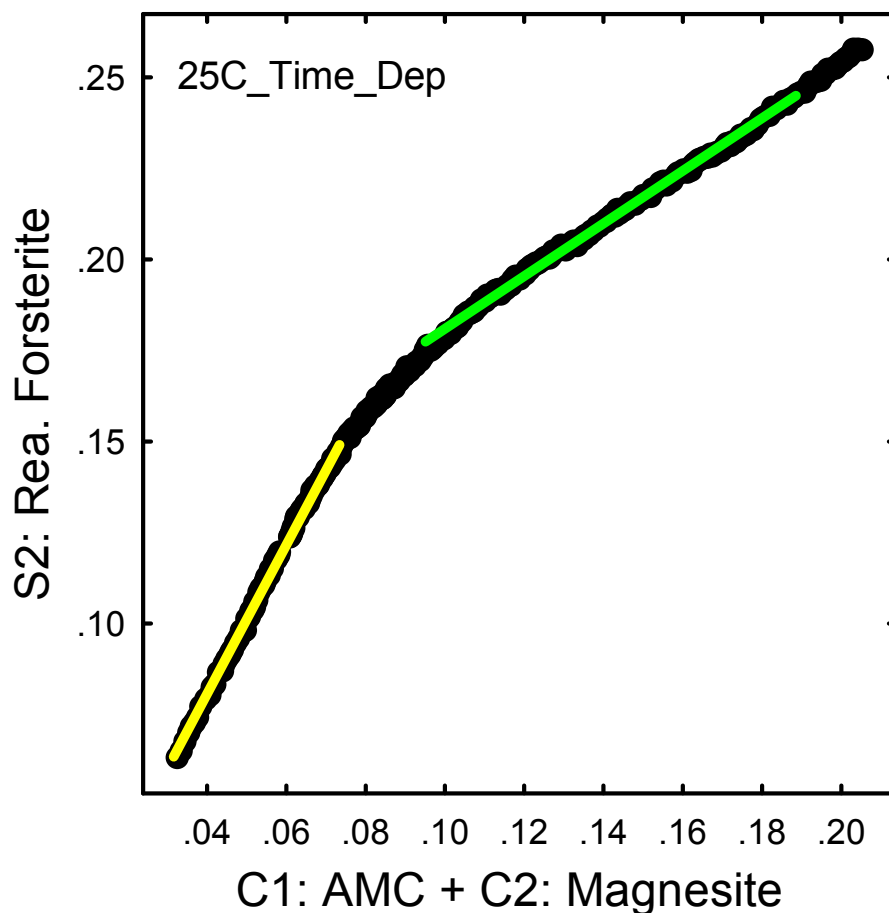


Figure S4. Data used to determine the ratio of the absorption coefficient of AMC to that of magnesite. This figure shows the relative concentration of component S2 versus the coadded relative concentrations of components C1 and C2 from chemometrics analyses of the ATR-IR spectra from experiment 25C_Time_Dep (see Table S1). Component S2 is assigned to reacted forsterite, and its concentration is from a MCR-ALS analysis of the ATR IR spectra in the SiO stretching region of amorphous SiO₂ (1060 to 1130 cm⁻¹) and forsterite (970 to 1060 cm⁻¹) as a function of time for 24 days after reaching 64% H₂O saturation (a H₂O coverage on forsterite of 1.82 ML; see Figure S2). Components C1 and C2 are assigned to AMC and magnesite, respectively (see Figure S3), and their concentrations are from a MCR-ALS analysis of the ATR IR spectra from experiment 25C_Time_Dep in CO deformation (715 to 770 cm⁻¹) and asymmetric CO stretching (1215 to 1600 cm⁻¹) regions of carbonate (see Figure S2). The data fit with the yellow line (from 0 to 160 hours) are from when AMC is growing in concentration, but before magnesite has nucleated (see Figure S2). The data fit with the green line (from 190 to 500 hours) are from when magnesite is growing in concentration, but the concentration of AMC has plateaued (see Figure S2). We assume that the absorption coefficient of reacted forsterite is the same, regardless if AMC or magnesite is the predominating carbonation product. Accordingly, the ratio of the absorption coefficient of AMC to that of magnesite is calculated by dividing the slope of the yellow line by that of the green line.

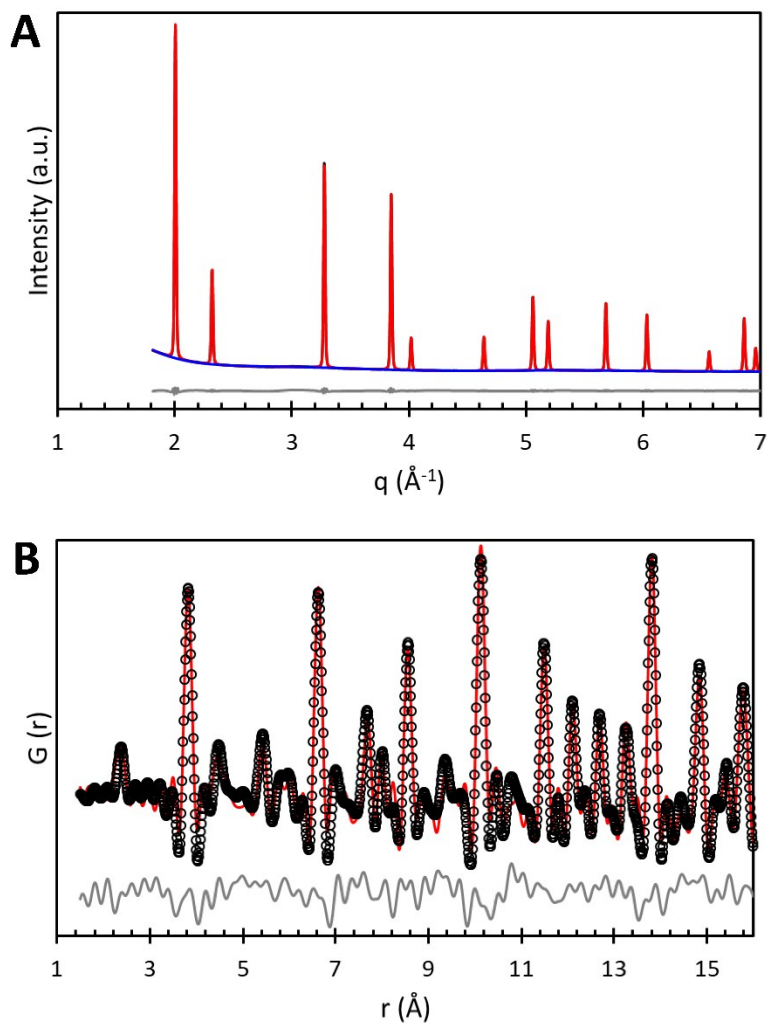


Figure S5. Instrument parameter measurements. (A) heXRD pattern of ceria standard (black) used to refine instrument parameters for Rietveld refinement. The calculated fit (red), background polynomial (blue), and residual (grey) were all calculated in GSAS-II. Gaussian peak parameters were refined to $u = 23.494$, $v = -0.306$, $w = 1.275$, and Lorentzian peak parameters were refined to $x = 0.731$, $y = 1.833$. (B) PDF pattern of ceria standard (black circles) used to refine instrument parameters $Q_{\text{damp}} = 0.04978$ and $Q_{\text{broad}} = 0.02239$. The fit (red) and residual (grey) were calculated in PDFgui with $R_w = 0.206173$ and reduced $\chi^2 = 0.00252237$.

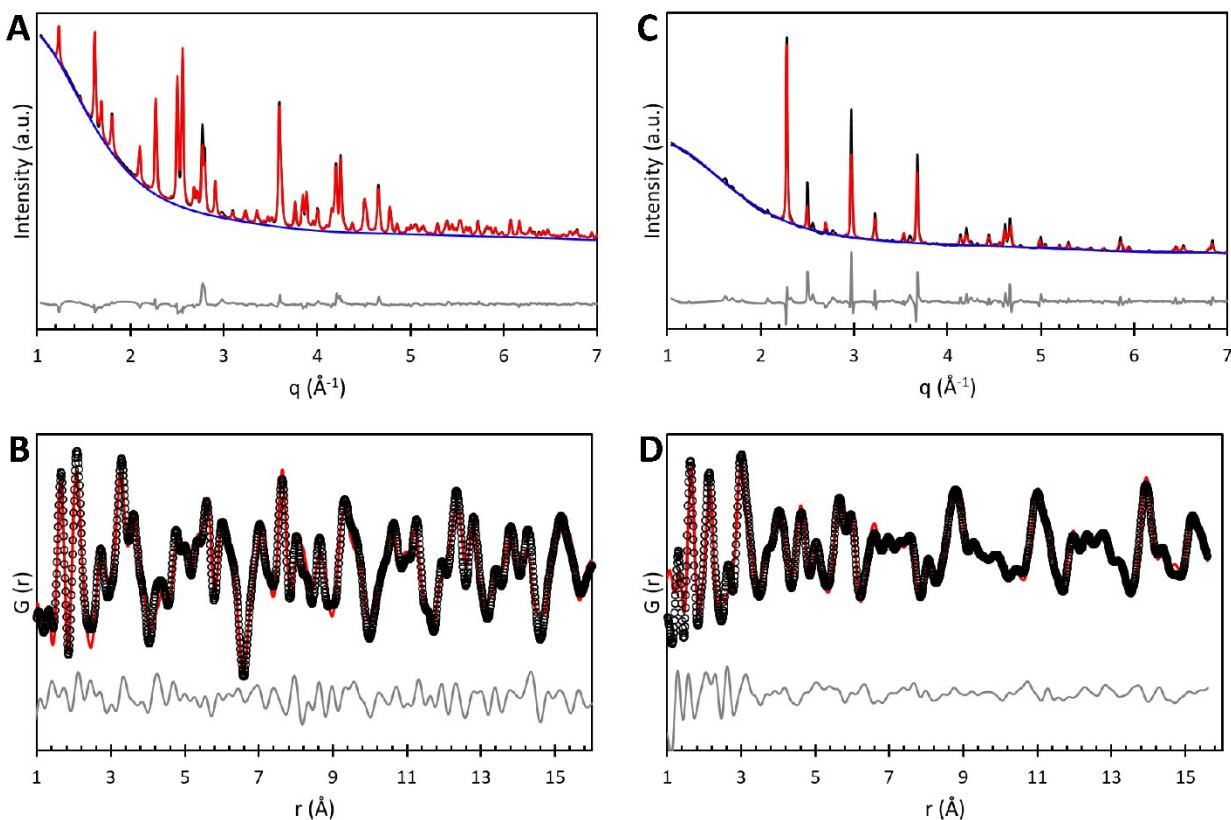


Figure S6. Rietveld fits of end-member compositions. (A) heXRD pattern of unreacted forsterite (black) used to refine the average domain size of 45 nm and sample microstrain of 1276. The calculated fit (red), background polynomial (blue), and residual (grey) were all calculated in GSAS-II with $R_{wp} = 2.28\%$, $R_F = 4.08\%$. (B) PDF pattern of unreacted forsterite (black circles) used to determine the unit cell parameters $a = 4.75556 \text{ \AA}$, $b = 10.1978 \text{ \AA}$, $c = 5.9843 \text{ \AA}$, $\alpha = \beta = \gamma = 90^\circ$. The fit (red) and residual (grey) were calculated in PDFgui with $R_w = 0.348197$ and $\chi^2 = 0.00284649$. (C) heXRD pattern of fully reacted forsterite (black) from experiment 50C_Fully_React (see Table S1) used to calculate magnesite particle sizes $> 3 \mu\text{m}$ and sample microstrain of 3176. The calculated fit (red), background polynomial (blue), and residual (grey) were all calculated in GSAS-II with $R_{wp} = 5.42\%$, $R_F = 9.38\%$. (D) PDF pattern of fully reacted forsterite (black circles) used to determine the magnesite unit cell parameters $a = b = 4.67013 \text{ \AA}$, $c = 15.1245 \text{ \AA}$, $\alpha = \beta = 90^\circ$, $\gamma = 120.4^\circ$. The fit (red) and residual (grey) were calculated in PDFgui with $R_w = 0.399462$ and $\chi^2 = 0.00143506$.

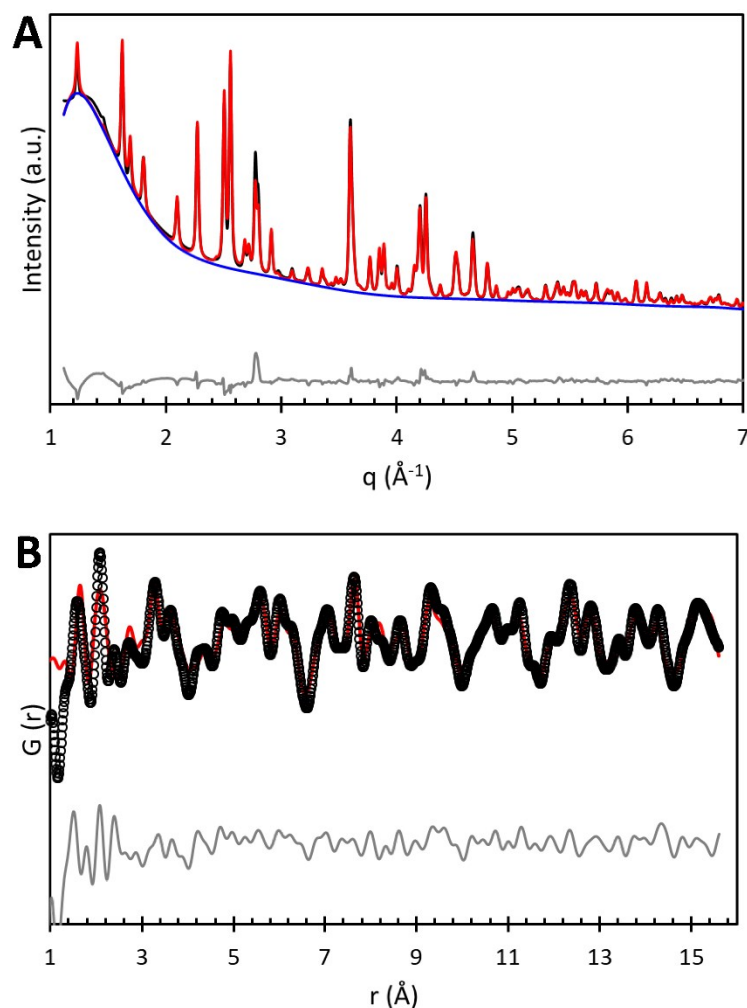


Figure S7. Rietveld refinement of the postreacted sample from titration 25C_Time_Dep. (A) heXRD pattern of sample (black), calculated fit (red), background polynomial (blue), and residual (grey) were all calculated in GSAS-II. Results of this fit are reported in Table S2 as “XRD Rietveld”. Forsterite domain size and microstrain were measured to be 45 nm and 1368, respectively, similar to the values refined for the starting material. Average magnesite domain size was determined to be 3.71 μm and a microstrain of 2919. The errors in fitting the structure factor is $R_F = 4.20\%$ for forsterite and $R_F = 4.98\%$ for magnesite. (B) PDF pattern of titration 25C_Time_Dep (black circles) with a refined fit (red) of 99.12 mol% forsterite and 0.88 mol% magnesite. Residuals are shown in grey; fits to PDF data were calculated in PDFgui with $R_w = 0.625982$ and $\chi^2 = 0.00204729$. Note: PDF residual using crystalline components only produces residual with an underestimated density of Mg-O distances (~ 2.2 \AA) and significant magnesite and forsterite features in the residual.

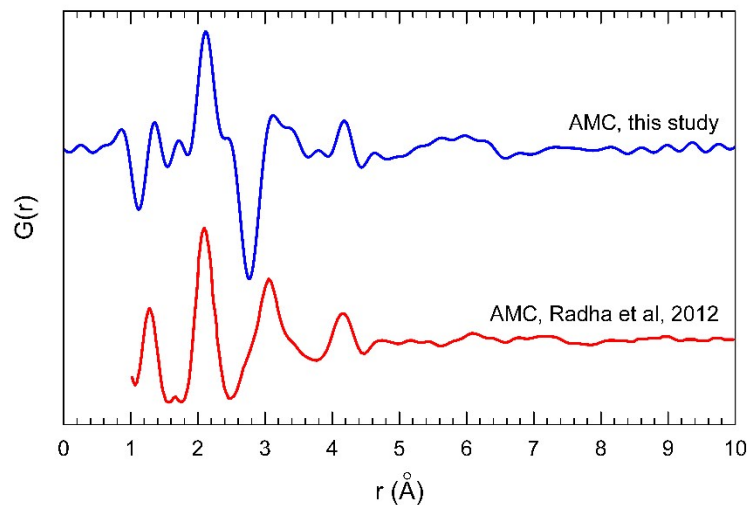


Figure S8. The PDF profiles of AMC reported in this study compared to the previously published structure by Radha et al., 2012.³⁰ Both AMC precipitates exhibit peaks at the C-O distance (~ 1.3 Å) and the Mg-O distance (~ 2.1 Å). The short-range order shows significant differences between the two structures, specifically between 2.2 and 3.5 Å. Most of these differences are likely attributable to a difference in AMC hydration. The AMC produced by Radha et al. was synthesized at high pH in bulk water and was measured to contain 1.28 water molecules per formula unit. The AMC in this study was produced under water-limited conditions, low pH conditions that are known to incorporate additional bicarbonate and only 0.8 water molecules per formula unit.²⁰

SI References

1. S. Brunauer, P. H. Emmett and E. Teller, *J. Am. Chem. Soc.*, 1938, **60**, 309-319.
2. O. Qafoku, E. S. Ilton, M. E. Bowden, L. Kovarik, X. Zhang, R. K. Kukkadapu, M. H. Engelhard, C. J. Thompson, H. T. Schaef, B. P. McGrail, K. M. Rosso and J. S. Loring, *J. Colloid Interface Sci.*, 2018, **515**, 129-138.
3. J. S. Loring, D. H. Bacon, R. D. Springer, A. Anderko, S. Gopinath, C. M. Yonkofski, C. J. Thompson, B. P. McGrail, K. M. Rosso and H. T. Schaef, *J. Chem. Eng. Data*, 2017, **62**, 1608-1614.
4. G. M. Bowers, H. T. Schaef, J. S. Loring, D. W. Hoyt, S. D. Burton, E. D. Walter and R. J. Kirkpatrick, *J. Phys. Chem. C*, 2017, **121**, 577-592.
5. C. J. Thompson, P. F. Martin, J. Chen, P. Benezeth, H. T. Schaef, K. M. Rosso, A. R. Felmy and J. S. Loring, *Rev. Sci. Instrum.*, 2014, **85**.
6. N. Spycher, K. Pruess and J. Ennis-King, *Geochim. Cosmochim. Acta*, 2003, **67**, 3015-3031.
7. S. Kerisit, E. J. Bylaska and A. Felmy, *Chem. Geol.*, 2013, **359**, 81-89.
8. S. Kerisit, J. H. Weare and A. R. Felmy, *Geochim. Cosmochim. Acta*, 2012, **84**, 137-151.
9. M. Boulet-Audet, T. Buffeteau, S. Boudreaault, N. Daugey and M. Pézolet, *J. Phys. Chem. B*, 2010, **114**, 8255-8261.
10. N. J. Harrick, *Internal Reflection Spectroscopy*, John Wiley & Sons, New York, 1967.
11. J. E. Bertie and H. H. Eysel, *Appl. Spectrosc.*, 1985, **39**, 392-401.
12. J. E. Bertie, S. L. Zhang and R. Manji, *Appl. Spectrosc.*, 1992, **46**, 1660-1665.
13. K. Ohta and H. Ishida, *Appl. Opt.*, 1990, **29**, 1952-1959.
14. J. S. Loring and D. P. Land, *Appl. Opt.*, 1998, **37**, 3515-3526.
15. H. A. Hans and F. K. Paul, *Am. Mineral.*, 1963, **48**, 124-137.
16. H. H. Adler and P. F. Kerr, *Am. Mineral.*, 1963, **48**, 839-853.
17. A. Gorzsás, *Open source MATLAB script from the Vibrational Spectroscopy Core Facility, Umeå University, Umeå Sweden*, 2017, <http://www.kbc.umu.se/english/visp/download-visp/>.
18. A. de Juan and R. Tauler, *Crit. Rev. Anal. Chem.*, 2006, **36**, 163-176.
19. M. Yeşilbaş and J.-F. Boily, *J. Phys. Chem. Lett.*, 2016, **7**, 2849-2855.
20. S. Leukel, M. Mondeshki and W. Tremel, *Inorg. Chem.*, 2018, **57**, 11289-11298.
21. E. Placencia-Gómez, S. N. Kerisit, H. S. Mehta, O. Qafoku, C. J. Thompson, T. R. Graham, E. S. Ilton and J. S. Loring, *Environ. Sci. Technol.*, 2020, **54**, 6888-6899.
22. A. Hoehner, S. Mergelsberg, O. J. Borkiewicz, P. M. Dove and F. M. Michel, *Acta Crystallographica Section A*, 2019, **75**, 758-765.
23. B. H. Toby and R. B. Von Dreele, *J. Appl. Crystallogr.*, 2013, **46**, 544-549.
24. D. Bostrom, *Am. Mineral.*, 1987, **72**, 965-972.
25. S. A. Markgraf and R. J. Reeder, *Am. Mineral.*, 1985, **70**, 590-600.
26. J. Liu, S. Pancera, V. Boyko, A. Shukla, T. Narayanan and K. Huber, *Langmuir*, 2010, **26**, 17405-17412.
27. A. Fernandez-Martinez, B. Kalkan, S. M. Clark and G. A. Waychunas, *Angew. Chem. Int. Ed.*, 2013, **52**, 8354-8357.
28. M. Saharay, A. O. Yazaydin and R. J. Kirkpatrick, *J. Phys. Chem. B*, 2013, **117**, 3328-3336.
29. Q. R. S. Miller, E. S. Ilton, O. Qafoku, D. A. Dixon, M. Vasiliu, C. J. Thompson, H. T. Schaef, K. M. Rosso and J. S. Loring, *J Phys Chem Lett*, 2018, DOI: 10.1021/acs.jpcclett.8b02162, 4988-4994.
30. A. V. Radha, A. Fernandez-Martinez, Y. Hu, Y.-S. Jun, G. A. Waychunas and A. Navrotsky, *Geochim. Cosmochim. Acta*, 2012, **90**, 83-95.